separations

MDPI

Article

Activating Peroxymonosulfate by a NovelFe-MOF-C/N Catalyst to Effectively Degrade Sulfamethoxazole: Catalyst Performance and Its Mechanism

Zhaowei Wu, Meiyi Hu, Pengfan Zhuo, Jie Wang and Shaoping Tong *

State Key Laboratory Breeding Base of Green Chemistry-Synthesis Technology, College of Chemical Engineering, Zhejiang University of Technology, Hangzhou 310014, China; wzw939579166@163.com (Z.W.); 221123010578@zjut.edu.cn (M.H.); zhuopengfan@163.com (P.Z.); wangj772022@163.com (J.W.)
* Correspondence: sptong@zjut.edu.cn; Tel./Fax: +86-571-88320960

Abstract: A composite Fe-MOF-C/N was prepared with Fe-MOF and g-C_3N_4 precursors, and its activation property of peroxymonosulfate (PMS) in the degradation of Sulfamethoxazole (SMX) was studied. XRD, SEM, and TEM analyses showed that Fe-MOF-C/N was porous and mainly composed of phases of Fe_3N, $C_{0.08}Fe_{1.92}$, and graphite. XPS indicated that Fe-MOF-C/N mainly had Fe, C, N, and O elements, among which Fe existed in the form of Fe^{2+} and Fe^{3+}. Fe-MOF-C/N was used to activate PMS to degrade SMX, and the result showed that Fe-MOF-C/N had excellent catalytic performance and 84.17% of SMX could be removed in 8 min. Free radical quenching experiments showed that $^1O_2$ was the main active species in Fe-MOF-C/N/PMS. The stability experiment showed that Fe-MOF-C/N had good stability, and the degradation rate of SMX only decreased by 5.8% after five times of use.

Keywords: peroxymonosulfate; MOFs; $C_{0.08}Fe_{1.92}$; sulfamethoxazole

Citation: Wu, Z.; Hu, M.; Zhuo, P.; Wang, J.; Tong, S. Activating Peroxymonosulfate by a NovelFe-MOF-C/N Catalyst to Effectively Degrade Sulfamethoxazole: Catalyst Performance and Its Mechanism. *Separations* **2024**, *11*, 356. https://doi.org/10.3390/separations11120356

Academic Editor: Grzegorz Boczkaj

Received: 27 November 2024
Revised: 17 December 2024
Accepted: 18 December 2024
Published: 21 December 2024

1. Introduction

The advanced oxidation technology of persulfate (PMS-AOP) has been widely applied in wastewater treatment and soil remediation because of its high efficiency [1,2]. PMS can be activated by various transition metals, of which cobalt-based catalysts are particularly effective, but pure cobalt catalysts face serious metal leakage and poor cycle performance. Among various catalysts, cobalt-based catalysts have good compatibility with PMS [3,4]. Persulfates, including peroxo sulfates (PMS) and peroxo disulfates (PDS), stand out among various oxidants due to their excellent stability and economy, making them the first choice in many applications. This preference is not only due to their own chemical properties, but also because they show great potential in environmental pollution control, water treatment, and other fields, especially in advanced oxidation processes (AOPs), where persulfate plays a vital role as an oxidizing agent [5–7]. Metal oxide catalysts, such as MFe_2O_4 (M@Co, Cu, Mn, and Zn) [8] MnO_2 [9], and Co_3O_4 [10], have been used for PMS activation. The catalysts in PMS-AOP reported so far still have some disadvantages like high-dose PMS and pH sensitivity, which need to be resolved.

Antibiotic drugs are widely used in clinical practice, thus leading to unexpected hazardous results. These ARGs and ARBs are not only able to persist in the environment, but can also be transmitted to humans through a variety of routes, such as the food chain, drinking water, or direct contact, posing a risk to human health [11]. The antibiotic can induce multiple AR via ROS-mediated genetic mutations and selective stress. Sulfamethoxazole (SMX), an antibiotic drug for the treatment of malaria, has been often detected in the environment. It is well known that SMX is harmful to organisms in water environments, affecting their growth and reproduction, and also leading to bacterial resistance. Asif et al. [12] pointed out in their study that the pollution of alga-derived organic matter

(AOM) during membrane distillation was mainly caused by protein-like substances. Hydroxyl radical (OH) and singlet oxygen ($^1O_2$) can be produced by activated peroxonosulfate (PMS), which significantly reduces the pollution of AOM in the membrane distillation process. Yan et al. [13] prepared CuO@Al_2O_3 (EPC) to activate persulfate to degrade SMX in water, and the removal rate of SMX was 99% within 2 h. Zhang et al. [14] synthesized $FeVO_4$ nanoribbons to construct a visible light-assisted PMS activation system for SMX degradation. It was found that the removal rate of SMX by PMS/$FeVO_4$/visible light was 3.9 times that of PMS/$FeVO_4$, 14.0 times that of PMS/visible light, and 14.1 times that of PMS alone. In these reports, although the removal rate of SMX is high, there still exist disadvantages like the large amount of the catalyst, a long reaction time, and pH dependence. Preparing a catalyst to activate persulfates works well, and there is still much room for development in the field of activating persulfates.

Based on the above facts, this study used Fe-MOF and g-C_3N_4 as precursors to prepare Fe-carbon/nitrogen (Fe-MOF-C/N) to activate PMS to degrade SMX. A series of characterization of Fe-MOF-C/N was carried out to verify its characteristics, and the reaction mechanism and possible degradation pathway of SMX by Fe-MOF-C/N/PMS were also discussed.

2. Experimental

2.1. Experimental Materials and Reagents

1,4-dicarboxybenzene, Melamine, NaOH, and H_2SO_4 were purchased from Shanghai Macklin Biochemical Technology Co., Ltd. (Shanghai, China).; methanol, ethanol, $FeCl_2 \cdot 4H_2O$, Furfuryl alcohol, and tert-Butanol were purchased from Shanghai Aladdin Biochemical Technology Co., Ltd. (Shanghai, China).; NaCl, $NaHCO_3$, K_2SO_4, DMF, SMX, and peroxymonosulfate were purchased from Shanghai Titan Scientific Co., Ltd. (Shanghai, China). All chemicals were analytically pure and were not treated prior to use. Deionized water was used throughout this study.

2.2. Characterization and Experimental Condition

X-Ray powder diffraction (XRD, Rigaku, SmartLab SE; Tokyo, Japan) was used to determine the crystal structures. X-Ray photoelectron spectroscopy (XPS, Kratos AXIS Ultra DLD) was conducted to analyze the elemental composition and chemical state. A Gemini 500 high-resolution transmission electron microscope (TEM, Carl Zeiss; Oberkochen, Germany) was used to detect the morphology of the catalyzer. The pH of solution was monitored by a pH-measuring apparatus (pH, Lei-ci (China), PHSJ-4F; Shanghai, China) during the whole experiment. The SMX content was detected by HPLC (Ultimate 3000 HPLC-Q; Waltham, MA, USA). The mobile phase was a mixture of acetonitrile, water, and triethylamine in a volume ratio of 200:799:1, and the pH of the mobile phase was adjusted with glacial acetic acid to 5.9. The ultraviolet absorption wavelength was 240 nm, and the flow rate was 1.0 mL/min. SEM (Zeiss Gemini Sigma 300 VP SEM; Oberkochen, Germany) was used to analyze and observe the surface morphology, microstructure, and chemical composition of catalyst materials.

The initial concentration of SMX solution was 50 mg/L, and was degraded in 250 mL beakers. Unless otherwise specified, the reaction system consisted of 200 mL SMX solution, 0.20 g/L PMS, and a suitable catalyst, and the initial pH of the solution was adjusted to the specified pH value with 0.1 M H_2SO_4 and NaOH solutions.

2.3. Preparation of Catalysts

2.3.1. Preparation of g-C_3N_4

The melamine was placed in a Muffle furnace and heated to 550 °C at a heating rate of 5 °C/min for 4 h. After cooling and grinding to powder, light yellow solid g-C_3N_4 was obtained.

2.3.2. Preparation of Fe-MOF

$FeCl_2 \cdot 4H_2O$ (0.8 g) and 1,4-dicarboxybenzene (2 g) were dissolved in 50 mL DMF, then loaded into 100 mL polytetrafluoroethylene inner tank, and placed in the reactor at 150 °C for 24 h. After cooling, the obtained precipitate was centrifuged from the solvent, washed and centrifuged with anhydrous methanol for 2 to 3 times, and dried in a vacuum oven at 80 °C for 4 h, and yellow powdered precursor Fe-MOF was obtained.

2.3.3. Preparation of Fe-MOF-C/N

Fe-MOF and g-C_3N_4 were dispersed in 10 mL anhydrous methanol, magnetically stirred at 500 r/min for 2 h, and then transferred to an 80 °C vacuum oven for 4 h to dry. The black powder catalyst Fe-MOF-C/N was obtained by calcination at 550 °C under nitrogen protection for 2 h. By changing the mass ratio of the precursor Fe-MOF to g-C_3N_4, the prepared catalysts were labeled Fe-MOF-C/N-1:0.3, Fe-MOF-C/N-1:0.5, Fe-MOF-C/N-1:0.7, and Fe-MOF-C/N-1:1.

3. Results and Discussion

3.1. Characteristic of Fe-MOF-C/N-1:0.5

The phase structure of the catalyst was determined by X-Ray diffraction (XRD), as shown in Figure 1. The diffraction peaks at 38.47°, 41.42°, 43.77°, 57.65°, and 69.32° suggested the appearance of Fe_3N (PDF#49-1663). The diffraction peaks at 44.02°, 44.84°, and 65.05° indicated the presence of the $C_{0.08}Fe_{1.92}$ (PDF#44-1291) phase. Peaks at 38.43°, 43.93°, and 45.47° were attributed to graphitic carbon (PDF#50-1082).

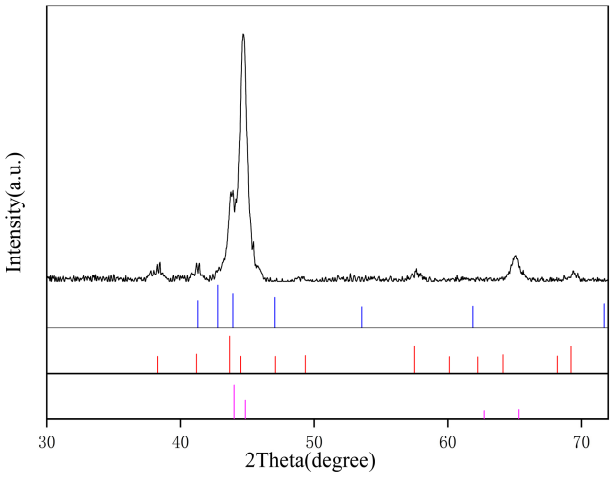

Figure 1. XRD spectra of Fe-MOF-C/N-1:0.5.

The SEM images of Fe-MOF-C/N before and after calcination (550 °C) are shown in Figure 2. Since the morphology and structure of the material may be changed before and after calcination, the morphology of Fe-MOF-C/N-1:0.5 was observed by SEM. The material presented a smooth surface before calcination (Figure 2a). After calcination (Figure 2b), the surface of Fe-MOF-C/N-1:0.5 presented dense micropores, which was due to the partial removal of the organic ligand at high temperature [15,16]. After calcination, the porous structure of the catalyst could expose more active sites, which was conducive to increasing the contact area between the catalyst and potassium bisulfate, thus improving the efficiency of the material activation of potassium bisulfate [16]. The element distributions of Fe-MOF-C/N-1:0.5 is shown in Figure 3. After calcination, C and N were distributed in similar positions. Fe was the brightest, followed by C and then N. However, the Fe content on the catalyst's surface was the highest and the distribution was wider.

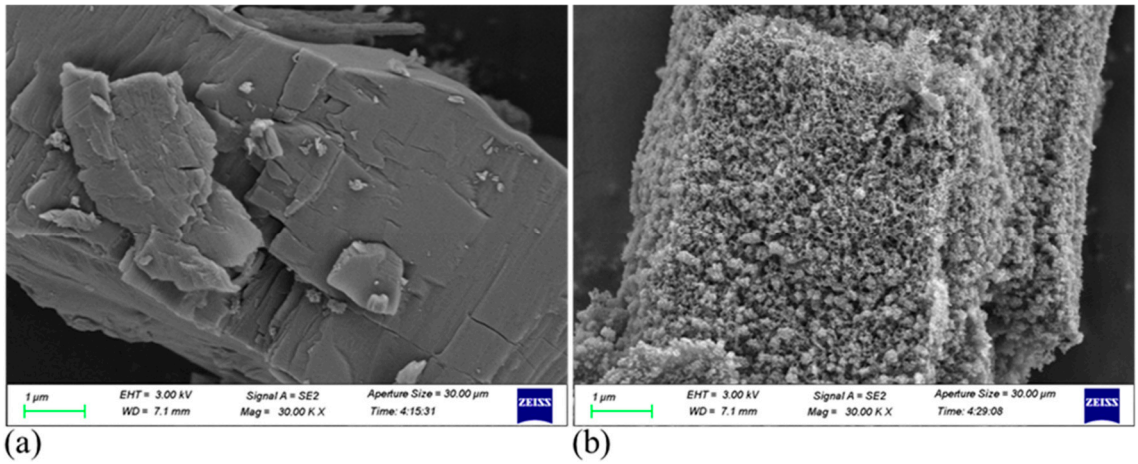

Figure 2. SEM of Fe-MOF-C/N-1:0.5 before (**a**) and after calcination (**b**).

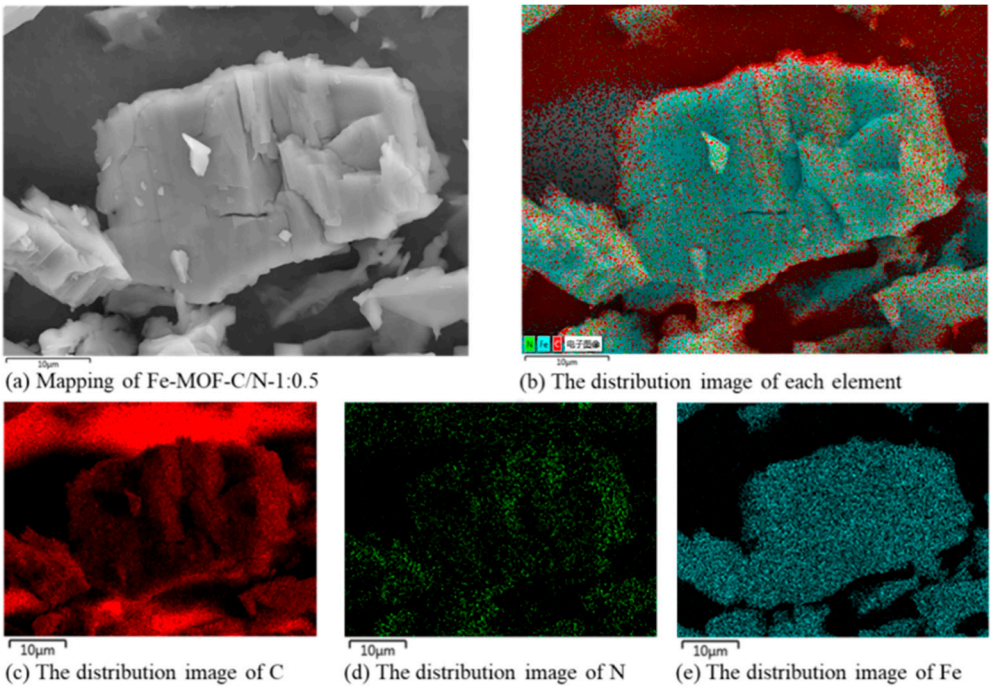

Figure 3. Mapping of Fe-MOF-C/N-1:0.5 after calcination (**a**); distribution of each element (**b**); distribution of C (**c**); distribution of N (**d**) and distribution of Fe (**e**).

The TEM image of Fe-MOF-C/N-1:0.5 is shown in Figure 4. It was found that the catalyst was coated with carbon. The lattice spacing in Figure 4c was 0.2056 nm, corresponding to the (200) crystal plane of $C_{0.08}Fe_{1.92}$. The lattice spacing of 0.2406 nm corresponded to the (111) crystal faces of Fe_3N (Figure 4d). Combined with XRD images, it could be seen that the catalyst contained $C_{0.08}Fe_{1.92}$ and Fe_3N.

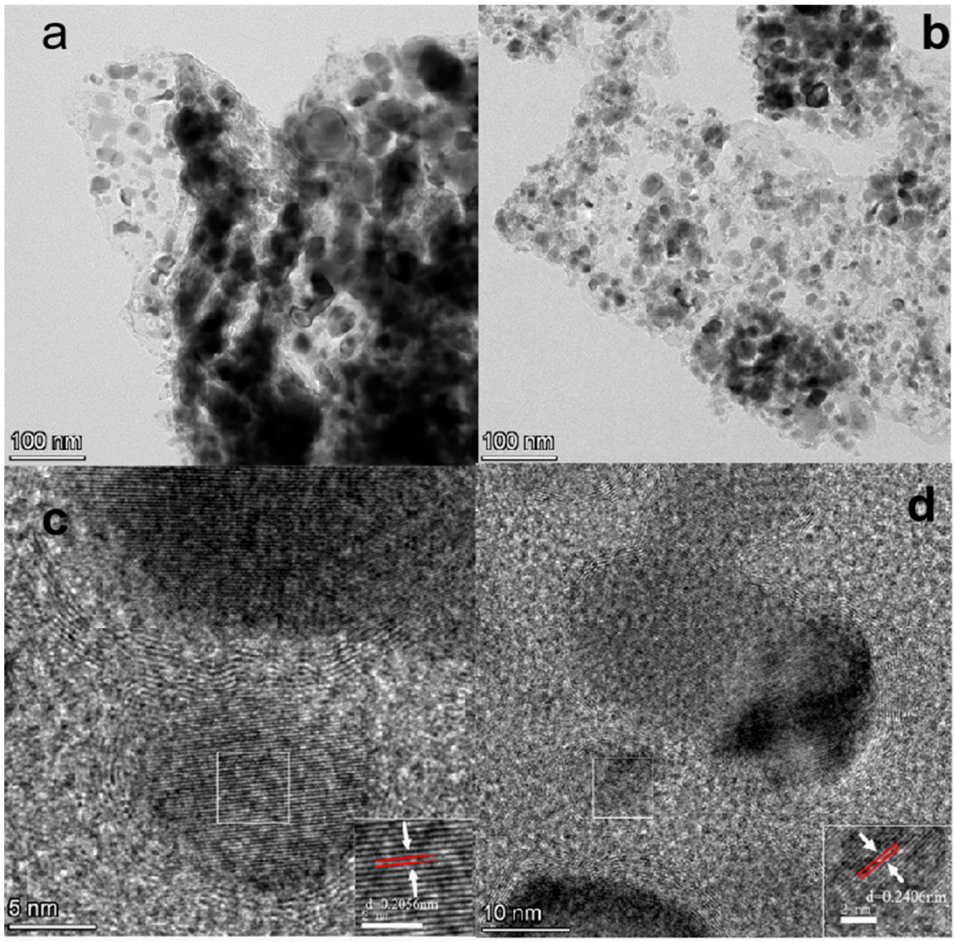

Figure 4. TEM image at 100 nm (**a,b**); TEM image with lattice spacing at 5 nm (**c**); TEM image with lattice spacing at 10 nm (**d**) of Fe-MOF-C/N-1:0.5.

The specific surface area and pore size parameters of the catalyst were obtained from the N_2 adsorption/desorption isothermal curve and pore size distribution diagram, respectively, as shown in Figure 5. The results indicated that the average pore diameter of Fe-MOF-C/N-1:0.5 was 15.1274 nm, the pore volume was 0.5595 cm^3/g, and the specific surface area was 149.01 m^2/g. The N_2 adsorption/desorption isotherm of Fe-MOF-C/N-1:0.5 was consistent with the typical type II adsorption/desorption isotherm, and the loop in the $0.4 < P/P_0 < 1.0$ range of the curve was also consistent with its porous structure.

The chemical composition of the prepared catalysts was determined by X-Ray photoelectron spectroscopy (XPS) and the results are shown in Figure 6. It could be seen that the catalyst was mainly composed of four elements: C, N, O, and Fe. The high-resolution spectrum of C-1s is shown in Figure 6b. Binding energies at 283.56 eV, 284.80 eV, 286.83 eV, and 289.76 eV represent C-Fe, C=C, C=O, and C-N, respectively [16–18]. The C-Fe bond also proved the presence of $C_{0.08}Fe_{1.92}$. Figure 6c shows the high-resolution spectrum of Fe-2p. The relative content of $2p_{3/2}$ and $2p_{1/2}$ orbits of Fe^{3+} were 19.79% (709.49 eV) and 20.05% (723.14 eV), respectively [19–22]. Both 705.86 eV (11.51%) and 706.63 eV (18.30%) belong to the $2p_{3/2}$ orbitals of Fe^{2+}, corresponding to Fe^{2+} in the Fe-C and Fe-N bonds, respectively [23–25]. 719.68 eV and 718.72 eV correspond to the $2p_{1/2}$ orbits of Fe^{2+}. Figure 6d shows the XPS spectrum of N-1s, in which the four peaks of 397.34 eV, 399.26 eV, 401.44 eV, and 403.16 eV correspond to Fe-N bond, pyrrole N, graphite N, and N oxide, respectively [22,25–28]. Combined with the distribution of elements in Figure 6a–d, XRD, and mapping, it was confirmed that Fe_3N and $C_{0.08}Fe_{1.92}$ were indeed present in the catalyst.

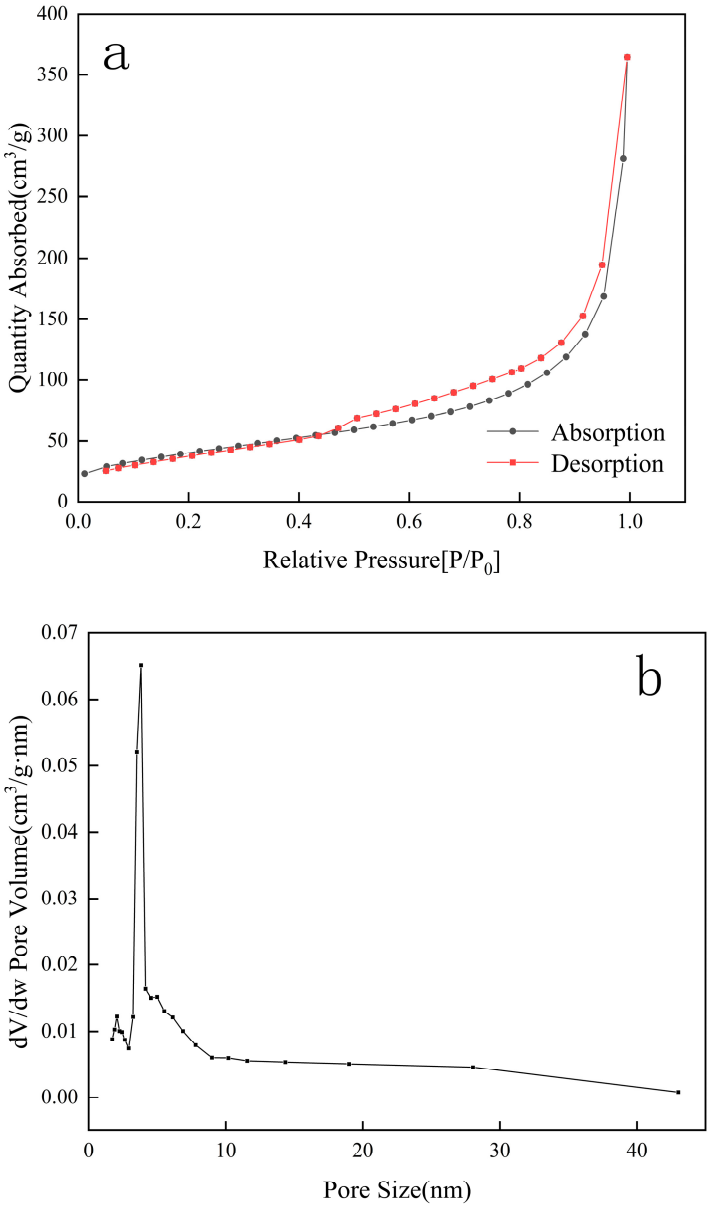

Figure 5. N_2 Absorption/desorption isotherms (**a**) and pore size distribution (**b**) of Fe-MOF-C/N-1:0.5.

3.2. Degradation of SMX in Fe-MOF-C/N-1:0.5/PMS System

The degradation of SMX in different systems is shown in Figure 7. The degradation rate of SMX in the PMS system was 18.91% in 8 min, and the adsorption degradation rate of Fe-MOF-C/N-1:0.5 for SMX was only 8.9%, indicating that PMS alone could not effectively oxidize SMX, and the adsorption effect of Fe-MOF-C/N-1:0.5 was not high. At the same time, the degradation rate of SMX in the Fe-MOF-C/N-1:0.5/PMS system was significantly increased to 84.17%.

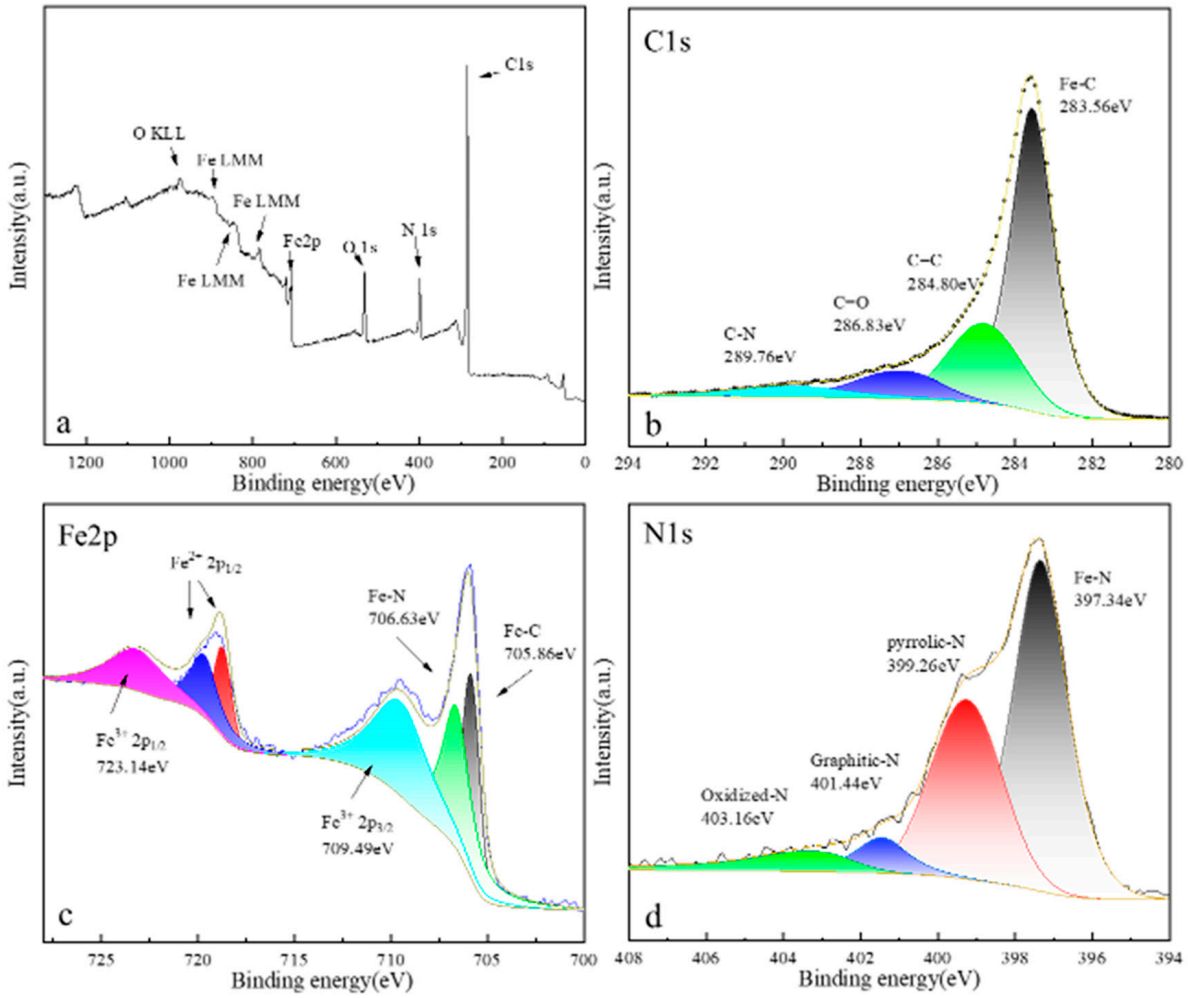

Figure 6. XPS spectra of Fe-MOF-C/N-1:0.5 (full spectrum (**a**) and high-resolution spectra of elements ((**b**) C, (**c**) Fe, and (**d**) N)).

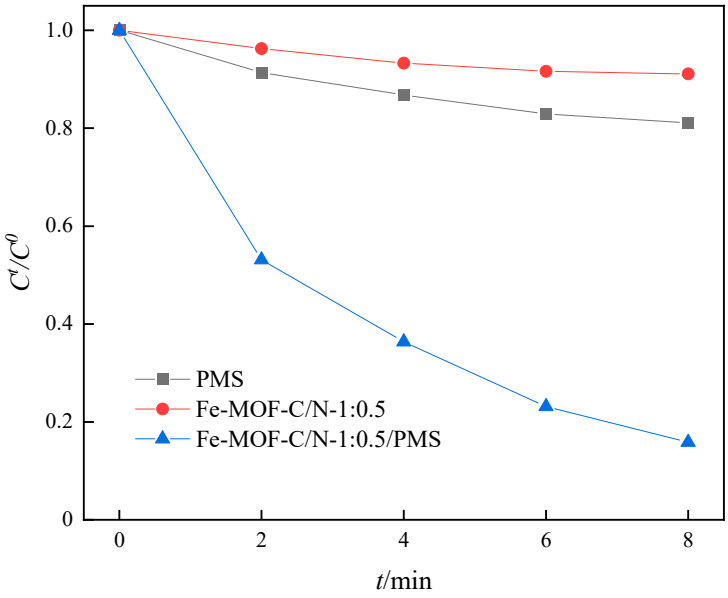

Figure 7. Efficiencies of Fe-MOF-C/N-1:0.5/PMS in degradation of SMX. Reaction conditions: SMX solution (200 mL 50 mg/L); PMS and Fe-MOF-C/N (0.20 g/L); pH = 7.

3.3. Effect of Fe-MOF and g-C_3N_4 Mass Ratio

In order to investigate the effect of the mass ratio of precursor Fe-MOF and g-C_3N_4 on the materials, Fe-MOF-C/N catalysts with different mass ratios were prepared, which were labeled as Fe-MoF-C/N-1:0.3, Fe-MOF-C/N-1:0.5, Fe-MOF-C/N-1:0.7, and Fe-MOF-C/N-1:1, respectively. The activation of PMS to degrade SMX was carried out under the same experimental conditions. As shown in Figure 8, the degradation rates of SMX in the presence of Fe-MOF-C/N-1:0.3, Fe-MOF-C/N-1:0.5, Fe-MOF-C/N-1:0.7, and Fe-MOF-C/N-1:1 were 60.47%, 83.54%, 76.75%, and 70.25%, respectively. With the increase in the proportion of g-C_3N_4, the active substances in the catalyst might be coated by carbon, thus reducing the degradation rate of SMX [29]. The reason for the low activity of Fe-MOF-C/N-1:0.3 might be that the content of g-C_3N_4 was too small, resulting in a low content of active substances in the catalyst after calcination [30,31]. The experimental results showed that the catalyst had the best performance when the mass ratio of Fe-MOF to g-C_3N_4 was 1:0.5.

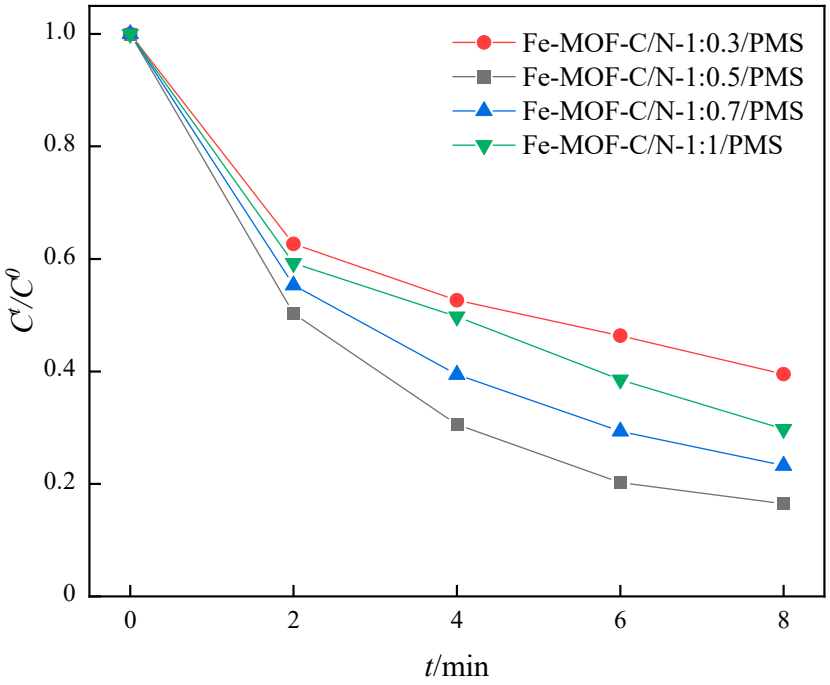

Figure 8. Effect of mass ratio of precursors on degradation efficiency of SMX. Reaction conditions: SMX solution (200 mL 50 mg/L); PMS and Fe-MOF-C/N (0.20 g/L); pH = 7.

3.4. The Effect of Calcination Temperature

In order to investigate the effect of calcination temperature, catalysts calcined at 550 °C, 600 °C, 700 °C, and 800 °C were prepared and labeled as Fe-MOF-C/N-1:0.5-550, Fe-MOF-C/N-1:0.5-600, Fe-MOF-C/N-1:0.5-700, and Fe-MOF-C/N-1:0.5-800. As shown in Figure 9, the degradation rates of SMX in the Fe-MOF-C/N-1:0.5-550/PMS and Fe-MOF-C/N-1:0.5-600/PMS systems were 83.54% and 81.35%, respectively, The degradation rates of SMX in the Fe-MOF-C/N-1:0.5-700/PMS and Fe-MOF-C/N-1:0.5-800/PMS systems were 74.35% and 61.72%, respectively. The experimental results showed that the catalyst had the best performance when the temperature of Fe-MOF-C/N was 550 °C.

The XRD spectra of the three catalysts prepared at 600 °C, 700 °C, and 800 °C are shown in Figure 10. The peaks of Fe-MOF-C/N-1:0.5-550 and Fe-MOF-C/N-1:0.5-600 were similar. Fe-MOF-C/N-1:0.5-700 only contained the characteristic peak of Fe_3C (PDF#89-2867) and Fe-MOF-C/N-1:0.5-800 only had the characteristic peak of Fe_3N (PDF#83-0876). However, the diffraction peak of $C_{0.08}Fe_{1.92}$ only appeared in Fe-MOF-C/N-1:0.5-550. These results indicate that the calcination temperature can affect the phase composition

of Fe-MOF-C/N-1:0.5, and $C_{0.08}Fe_{1.92}$ might be the reason for the better performance of Fe-MOF-C/N-1:0.5.

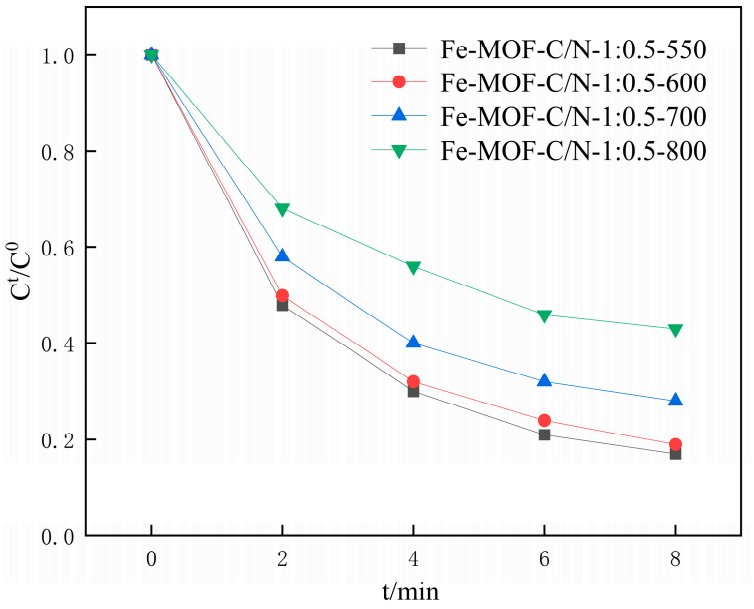

Figure 9. Effect of calcination temperature on degradation of SMX. Reaction conditions: SMX solution (200 mL 50 mg/L); PMS and Fe-MOF-C/N (0.20 g/L); pH = 7.

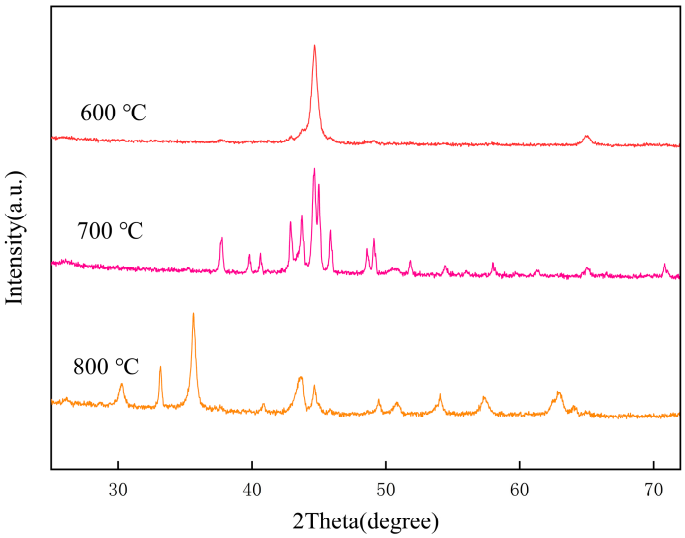

Figure 10. XRD spectra of Fe-MOF-C/N-1:0.5 prepared at different calcination temperatures.

3.5. Mechanism

In the PMS-AOPs system, ·OH, SO_4^-, and $^1O_2$ might be active substances in the degradation of organic matter [32,33]. Tert-butanol (TBA) can react with OH ($k = 3.8 - 7.6 \times 10^8$ $M^{-1}s^{-1}$) and was used as a free radical scavenger of OH [34]. Ethanol can be used as a quenching agent for OH and SO_4^-. The contribution of ·OH and SO_4^- in SMX degradation could be determined by adding tert-butanol and ethanol to the solution [35,36]. Furfuryl alcohol (FA) could effectively quench $^1O_2$ in the solution [37]. It can be seen from Figure 11 that $^1O_2$ had the greatest effect on SMX degradation, while ·OH and SO_4^- had little effect on SMX degradation.

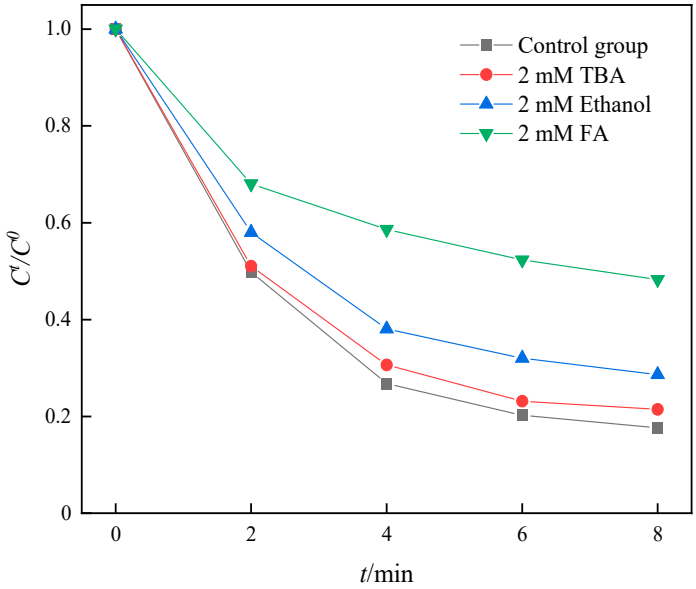

Figure 11. Effect of ethanol, TBA, and FFA on degradation of SMX. Reaction conditions: SMX solution (200 mL 50 mg/L); PMS and Fe-MOF-C/N (0.20 g/L); pH = 7.

Combined with the reported studies, the mechanism of this system may be shown in Equations (1)–(7) [38–40]: (1) In the catalyst, Fe(II) breaks the O-O bond of HSO_5^- to form SO_4^- and Fe(III), and SO_4^- can directly degrade organic matters or react with H_2O to form ·OH. (2) Fe(III) reacts with PMS to form Fe(II) and SO_5^-, and then SO_5^- reacts to form SO_4^- and $^1O_2$. (3) Fe(II) activates PMS to directly generate O_2^-, and then $\cdot O_2^-$ generates $^1O_2$.

$$Fe(II) + HSO_5^- \rightarrow Fe(III) + SO_4^- + OH^- \quad (1)$$

$$SO_4^- + H_2O \rightarrow SO_4^{2-} + \cdot OH + H^+ \quad (2)$$

$$Fe(III) + HSO_5^- \rightarrow Fe(II) + SO_5\cdot^- + H^+ \quad (3)$$

$$2SO_5\cdot^- \rightarrow 2SO_4\cdot^- + {}^1O_2 \quad (4)$$

$$Fe(II) + HSO_5^- \rightarrow Fe(III) + HSO_4^- + \cdot O_2^- \quad (5)$$

$$\cdot O_2^- + H^+ \rightarrow \cdot HO_2 \quad (6)$$

$$\cdot O_2^- + \cdot HO_2 \rightarrow {}^1O_2 + HO_2^- \quad (7)$$

3.6. The Effect of pH

The pH of solution will have a certain influence on the production of free radicals in the activation of PMS. SO_4^- could react with OH^- to form OH under neutral or alkaline conditions [41]. As shown in Figure 12, as the initial pH of the solution increased from 5.0 to 9.0, the degradation rates of SMX did not change significantly, being 81.42%, 86.84%, and 84.17%, respectively. The dissolution of Fe in water with an initial pH of 5.0, 7.0, and 9.0 was determined by ICP-OES/MS, which was 0.8252 mg/L, 0.5938 mg/L, and 0.6153 mg/L, respectively. This suggested that most Fe dissolved in acidic solutions, as the chemical bonds between metal centers and organic ligands might be more easily broken under acidic conditions. However, the final results showed that the catalyst was less affected by the pH value of the solution.

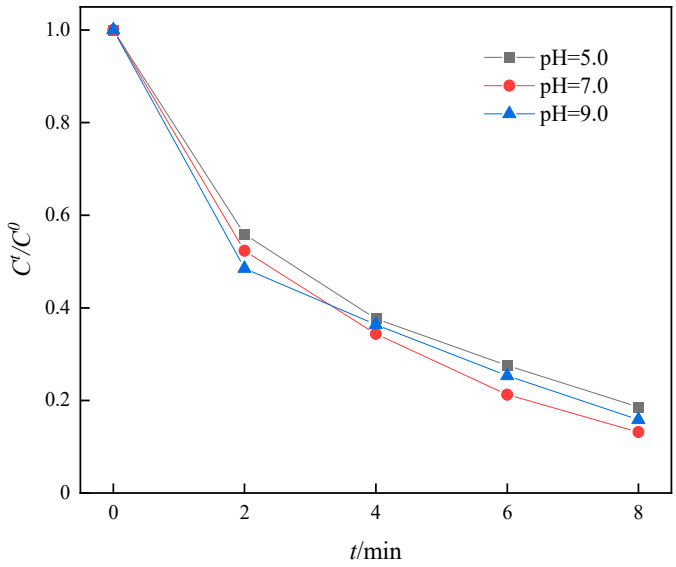

Figure 12. Effect of different initial pH values on degradation efficiency of SMX. Reaction conditions: SMX solution (200 mL 50 mg/L); PMS and Fe-MOF-C/N (0.20 g/L); pH = 7.

3.7. The Effect of PMS Dosage

As the dosage difference in PMS will affect the reaction cost and might affect the degradation efficiency, degradation experiments were performed. As shown in Figure 13, when the dosage of Fe-MOF-C/N-1:0.5 was 0.20 g/L, the degradation rate of SMX gradually increased with the increase in the dosage of PMS. When PMS was increased from 0.30 g/L to 0.40 g/L, the degradation rate of SMX was not significantly improved; perhaps the PMS of utilization rate was close to the limit when the PMS is 0.30 g/L.

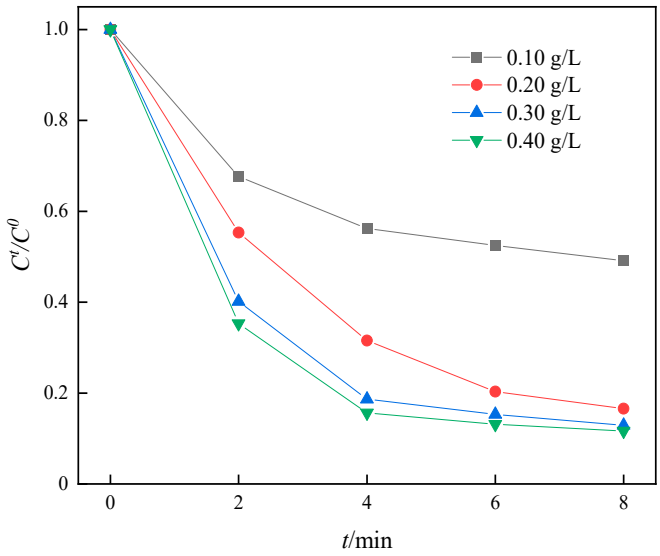

Figure 13. Effect of different dosage of PMS on degradation efficiency of SMX. Reaction conditions: SMX solution (200 mL 50 mg/L) and Fe-MOF-C/N (0.20 g/L); pH = 7.

3.8. The Effect of Fe-MOF-C/N-1:0.5 Dosage

Too little catalyst dosing will result in PMS not being fully activated, reducing the utilization of PMS and the degradation rate of SMX; too much will result in catalyst wastage, increasing the cost, as well as removing SO_4^- [42].

$$Fe^{2+} + SO_4^- \rightarrow Fe^{3+} + SO_4^{2-} \quad (8)$$

As shown in Figure 14, when the PMS dosage was 0.20 g/L, the degradation rates of SMX were 60.21%, 76.86%, 85.62%, and 88.60%, respectively, as the Fe-MOF-C/N-1:0.5 dosage was elevated from 0.10 to 0.40 g/L. And within 2 min, the higher the catalyst dosage was, the faster the SMX content in the solution decreased, which indicated that the dosage of the catalyst affects the degradation rate of the organic matter in the solution. In addition, the adsorption effect of Fe-MOF-C/N-1:0.5 on SMX is shown in Figure 15, and the SMX removal rate increased with the rise in catalyst dosage. Based on the above results, the optimal dosages of PMS and Fe-MOF-C/N-1:0.5 for the activation of PMS for SMX degradation were 0.30 g/L and 0.40 g/L, respectively.

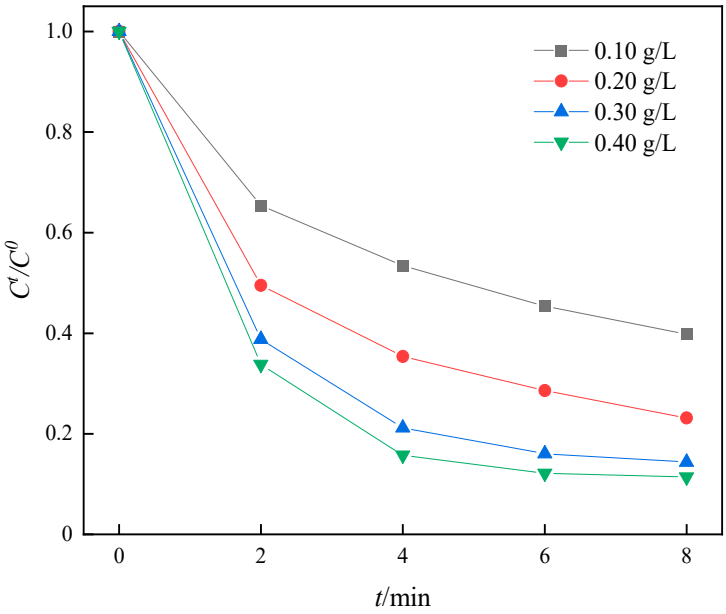

Figure 14. Effect of different dosage of Fe-MOF-C/N-1:0.5 on degradation of SMX. Reaction conditions: SMX solution (200 mL 50 mg/L) and PMS (0.20 g/L).

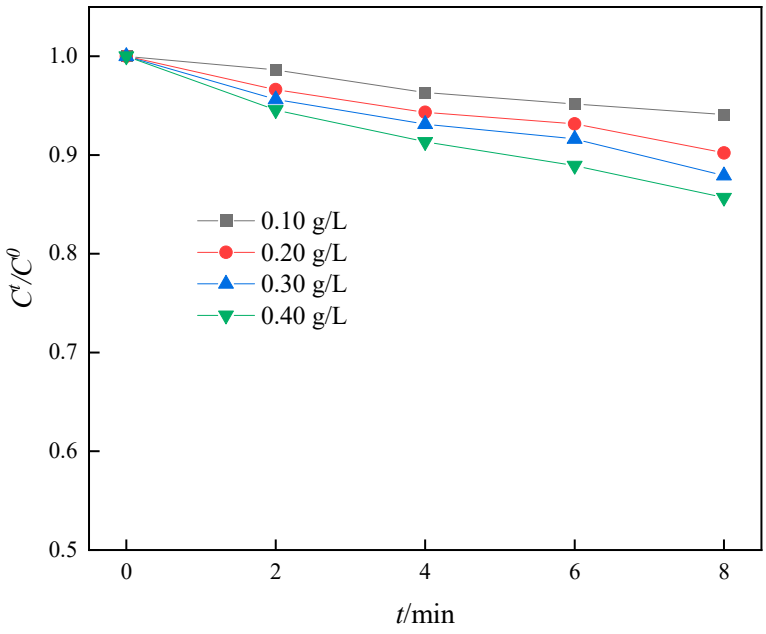

Figure 15. The adsorption effect of different Fe-MOF-C/N-1:0.5 dosages on SMX. Reaction conditions: SMX solution (200 mL 50 mg/L) and PMS (0.20 g/L).

3.9. Recycling Test

Cyclic experiments were carried out to degrade SMX, and the experimental results are shown in Figure 16. From the first to the fifth experiment, the degradation rates of SMX were 85.42%, 83.42%, 80.79%, 79.56%, and 77.63%, respectively, and the degradation rates of SMX decreased by 7.79% (Figure 16). And there was no significant difference between the XRD patterns of the catalysts before and after use (Figure 17), so Fe-MOF-C/N-1:0.5 could be considered to have a stable structure.

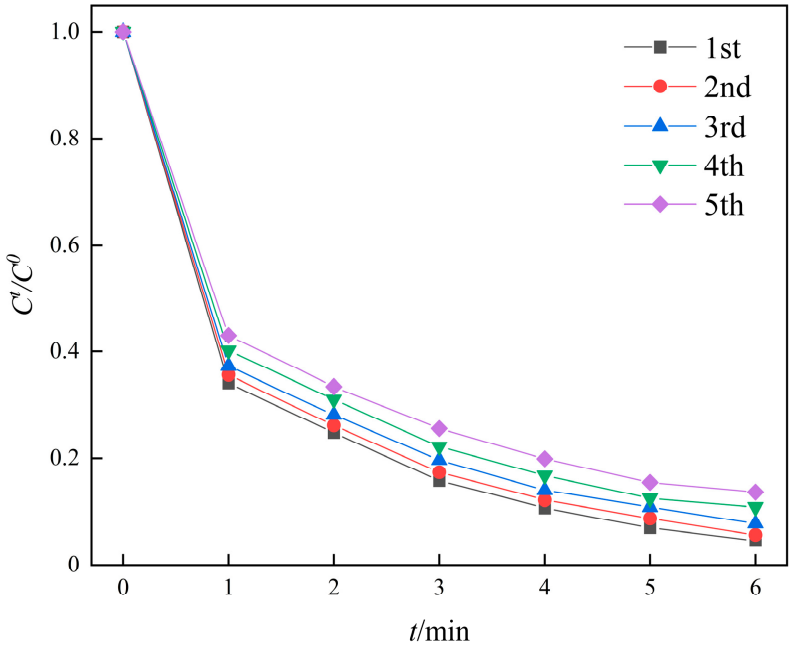

Figure 16. Recycling test of Fe-MOF-C/N-1:0.5 for activating PMS. Reaction conditions: SMX solution (200 mL 50 mg/L); PMS and Fe-MOF-C/N (0.20 g/L).

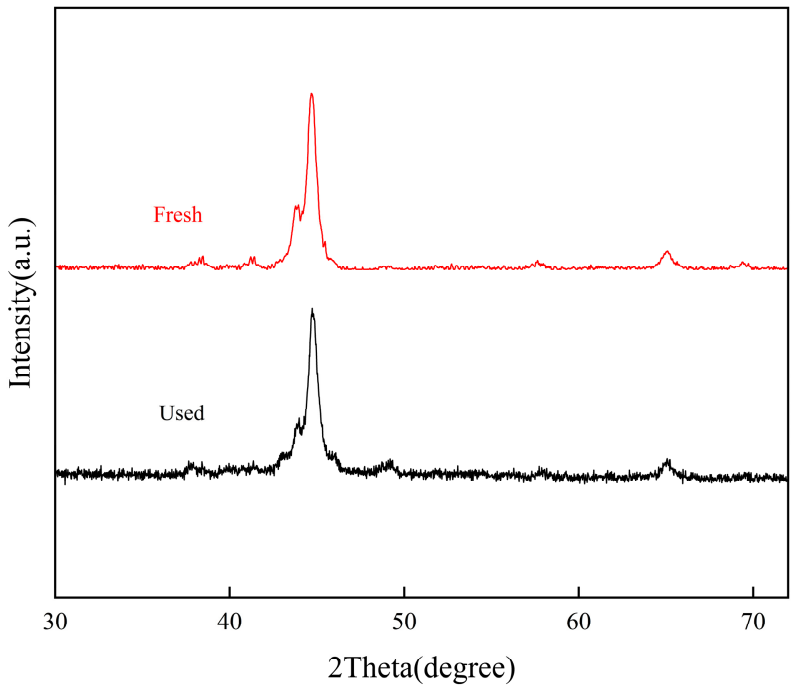

Figure 17. XRD of fresh and used catalysts.

3.10. Intermediate Product of SMX

After the detection and analysis of the intermediates in the degradation of SMX, eleven intermediates with a high peak intensity of mass spectrum except SMX were preliminarily identified. ROS mainly attacked the S-N bond of SMX in the system, -NH_2 in the benzene ring, and the β-carbon in the amino position [43]. Based on this, the possible degradation pathway of SMX in the Fe-MOF-C/N-1:0.5/PMS system is shown in Figure 18. The pathway involved ring opening, dehydrogenation, decarbonization, oxidation, rearrangement, and other chemical reactions [44,45].

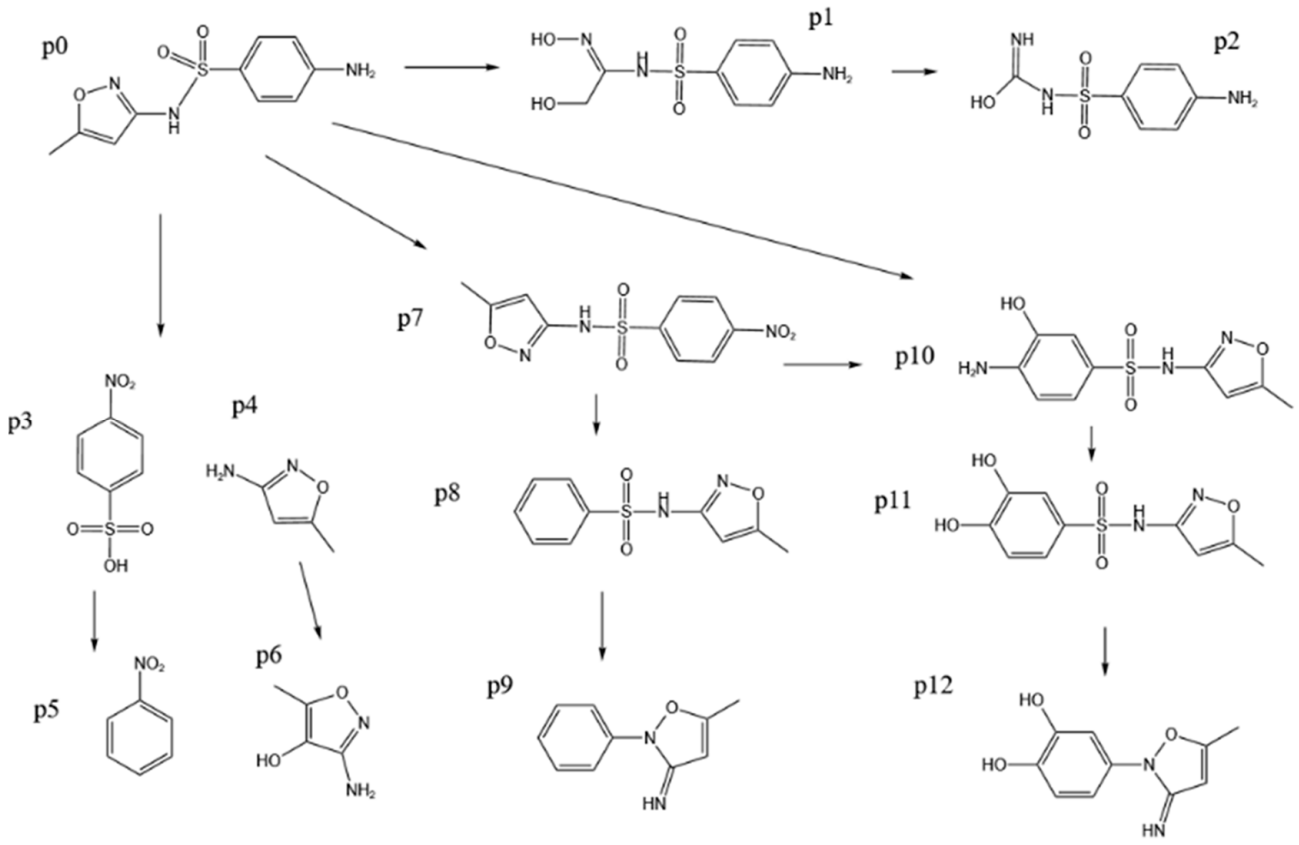

Figure 18. Possible degradation pathway of SMX.

The degradation of SMX may produce toxic intermediates. Figure 19 represents the lethal concentrations of the substances to large daphnia and fat-head fish, as well as their respective developmental toxicity and mutagenicity. Most intermediates of SMX had no or lower developmental toxicity than SMX itself, and p6 and p9 had certain mutagenicity. The lethal concentrations of intermediate p3 and p4 with high toxicity were less than 10 mg/L, but lower than that of SMX. The lethal concentrations of p8, p10, p11, and p12 were less than 3 mg/L, which was slightly more toxic than SMX itself. Overall, the system can degrade SMX, making it less toxic to the environment and beneficial to aquatic organisms.

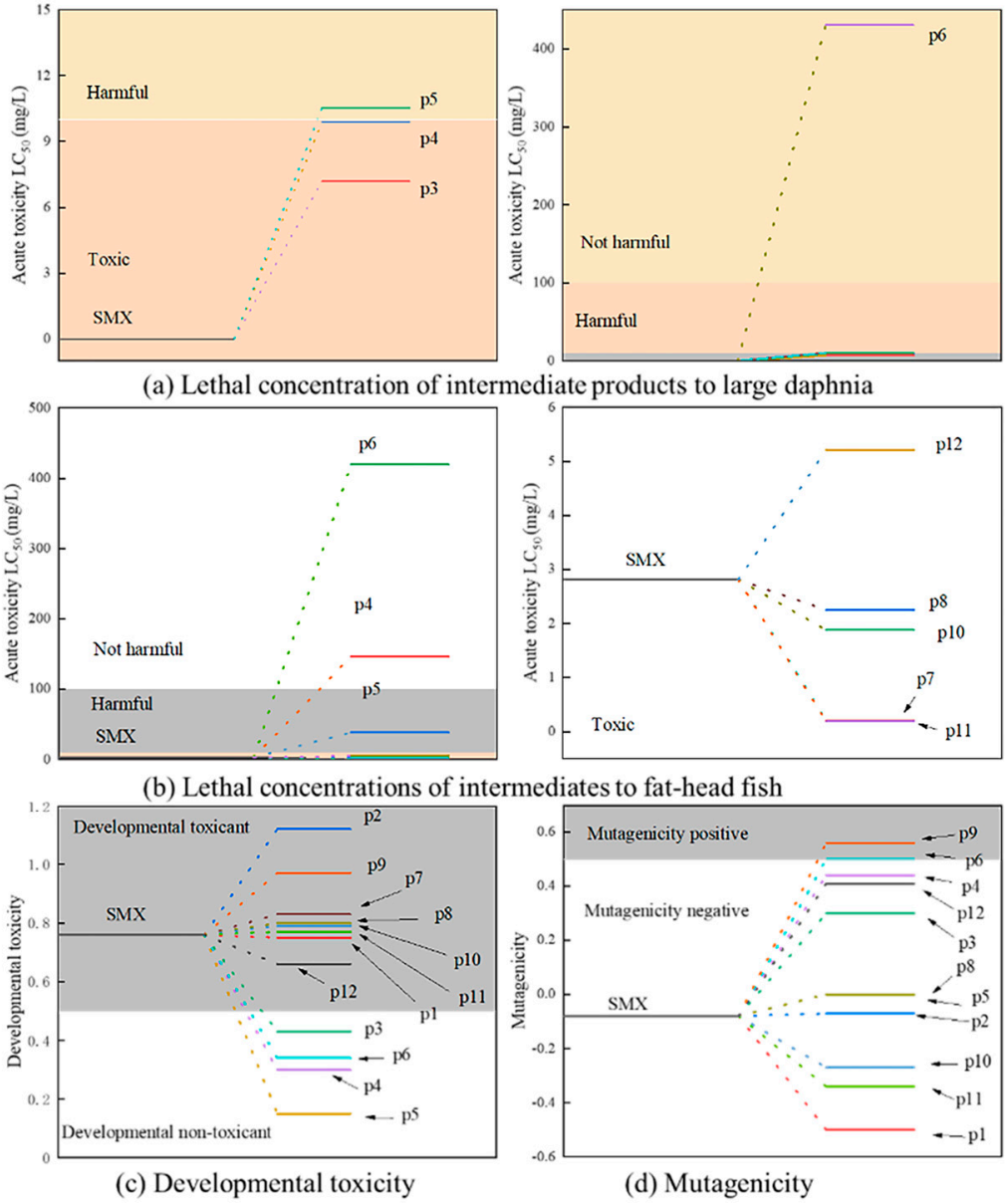

Figure 19. Toxicity analysis of intermediate products of SMX, Lethal concentrations of intermediates products to large dophnia (**a**); Lethal concentrations of intermediates to fat-heat fish (**b**); Developmental toxicity (**c**); Mutagenicity (**d**).

4. Conclusions

(1) Fe-MOF-C/N was prepared with precursors of Fe-MOF and g-C_3N_4. It had good performance in the activation of peroxymonosulfate (PMS) to degrade Sulfamethoxazole (SMX) and stability in a wide initial pH range.

(2) The experimental results showed that the composite had the best catalytic activity when the mass ratio of Fe-MOF to g-C_3N_4 was 1:0.5 (Fe-MOF-C/N-1:0.5) and the optimum calcination temperature was 550. The optimal dosages of PMS and Fe-MOF-C/N-1:0.5 for the activation of PMS for SMX degradation were 0.30 g/L and 0.40 g/L, respectively.

(3) The results of XRD, XPS, SEM, BET, and TEM indicated that it had a porous structure and was mainly composed of Fe_3N, $C_{0.08}Fe_{1.92}$, and graphitic carbon.

(4) The free radical quenching experiment confirmed that $^1O_2$ in PMS/Fe-MOF-C/N-1:0.5 was the main substance to degrade SMX. Most intermediates of SMX had no or lower developmental toxicity than SMX itself, which had benefits to the environment and organisms.
(5) The Fe-MOF-C/N catalyst has high catalytic activity in the activation of persulfate. The catalytic activity of Fe-MOF-C/N is insensitive to the pH value of the solution, thus leading to its excellent application significance.

Author Contributions: Conceptualization, S.T. and Z.W.; methodology, S.T.; software, M.H.; validation, P.Z., M.H. and J.W.; formal analysis, J.W.; investigation, P.Z.; resources, M.H.; data curation, Z.W.; writing—original draft preparation, S.T.; writing—review and editing, Z.W.; visualization, M.H.; supervision, P.Z.; project administration, S.T.; funding acquisition, J.W. All authors have read and agreed to the published version of the manuscript.

Funding: This research received no external funding.

Data Availability Statement: No new data were created.

Conflicts of Interest: The authors declare no conflict of interest.

References

1. Barrios-Bermúdez, N.; Cerpa-Naranjo, A.; Rojas-Cervantes, M. Efficient Methylene Blue Degradation by Activation of Peroxymonosulfate over Co(II) and/or Fe(II) Impregnated Montmorillonites. *Catalysts* **2024**, *14*, 479. [CrossRef]
2. Nikitin, D.; Kaur, B.; Preis, S.; Dulova, N. Degradation of Antibiotic Vancomycin by UV Photolysis and Pulsed Corona Discharge Combined with Extrinsic Oxidants. *Catalysts* **2023**, *13*, 466. [CrossRef]
3. Zhou, X.; Li, X.; Xu, C.; Yang, L.; Yang, G.; Guo, L. A persulfate oxidation system for removing acid orange from aqueous solution: Evaluation and degradation mechanism. *J. Environ. Manag.* **2022**, *322*, 116054. [CrossRef] [PubMed]
4. Liu, J.; Kang, X.; Li, D.; Sun, Z.; Song, X.; Zhao, X. Degradation of imidacloprid in water by $ZnCo_2O_4$ activated peroxymonosulfate system. *Chin. J. Environ. Eng.* **2021**, *15*, 1227–1241.
5. Matzek, L.; Carter, K. Activated persulfate for organic chemical degradation: A review. *Chemosphere* **2016**, *151*, 178–188. [CrossRef] [PubMed]
6. Ghanbari, F.; Moradi, M. Application of peroxymonosulfate and its activation methods for degradation of environmental organic pollutants. *Chem. Eng. J.* **2017**, *310*, 41–62. [CrossRef]
7. Ding, M.; Ao, W.; Xu, H.; Chen, W.; Tao, L.; Shen, Z.; Liu, H.; Lu, C.; Xie, Z. Facile construction of dual heterojunction $CoO@TiO_2$/MXene hybrid with efficient and stable catalytic activity for phenol degradation with peroxymonosulfate under visible light irradiation. *J. Hazard. Mater.* **2021**, *420*, 126686. [CrossRef] [PubMed]
8. Saputra, E.; Muhammad, S.; Sun, H.; Patel, A.; Shukla, P.; Zhu, Z.H.; Wang, S. α-MnO_2 activation of peroxymonosulfate for catalytic phenol degradation in aqueous solutions. *Catal. Commun.* **2012**, *26*, 144–148. [CrossRef]
9. Ren, Y.; Lin, L.; Ma, J.; Yang, J.; Feng, J.; Fan, Z. Sulfate radicals induced from peroxymonosulfate by magnetic ferrospinel MFe_2O_4 (M=Co, Cu, Mn, and Zn) as heterogeneous catalysts in the water. *Appl. Catal. B Environ.* **2015**, *165*, 572–578. [CrossRef]
10. Deng, J.; Feng, S.; Zhang, K.; Li, J.; Wang, H.; Zhang, T.; Ma, X. Heterogeneous activation of peroxymonosulfate using ordered mesoporous Co_3O_4 for the degradation of chloramphenicol at neutral, pH. *Chem. Eng. J.* **2017**, *308*, 505–515. [CrossRef]
11. Miao, S.; Zhang, Y.; Li, B.; Yuan, X.; Men, C.; Zuo, J. Antibiotic intermediates and antibiotics synergistically promote the development of multiple antibiotic resistance in antibiotic production wastewater. *J. Hazard. Mater.* **2024**, *479*, 135601. [CrossRef]
12. Asif, M.; Ji, B.; Maqbool, T.; Zhang, Z. Algogenic organic matter fouling alleviation in membrane distillation by peroxymonosulfate (PMS): Role of PMS concentration and activation temperature. *Desalination* **2021**, *516*, 115225. [CrossRef]
13. Yan, J.; Li, J.; Peng, J.; Zhang, H.; Zhang, Y.; Lai, B. Efficient degradation of sulfamethoxazole by the $CuO@Al_2O_3$ (EPC) coupled PMS system: Optimization, degradation pathways and toxicity evaluation. *Chem. Eng. J.* **2019**, *359*, 1097–1110. [CrossRef]
14. Zhang, J.; Zhao, W.; Li, Z.; Lu, C.; Zhu, M. Visible-light-assisted peroxymonosulfate activation over Fe(II)/V(IV) self-doped $FeVO_4$ nanobelts with enhanced sulfamethoxazole degradation: Performance and mechanism. *Chem. Eng. J.* **2021**, *403*, 126384. [CrossRef]
15. Wang, Z.; Laddha, G.; Kanitkar, S.; Spivey, J. Metal organic framework-mediated synthesis of potassium-promoted cobalt-based catalysts for higher oxygenates synthesis. *Catal. Today* **2017**, *298*, 209–215. [CrossRef]
16. Li, Y.; Zhang, Z.; Zhang, L.; Li, Y.; Lin, K.; Tong, S. Preparation of metal organic frame derived MgO-porous carbon composite and its high catalytic activity in ozonation with excellent stability. *J. Taiwan Inst. Chem. Eng.* **2024**, *156*, 105339. [CrossRef]
17. Ju, J.; Kim, M.; Jang, S.; Kim, Y.; Choi, Y.; Baeck, S.; Shim, S. 3D in-situ hollow carbon fiber/carbon nanosheet/$Fe_3C@Fe_3O_4$ by solventless one-step synthesis and its superior supercapacitor performance. *Electrochim. Acta* **2017**, *252*, 215–225. [CrossRef]
18. Xu, H.; Ma, W.; Zhang, T.; Hu, Y.; Du, G.; Yang, H.; Li, Y.; Xu, Y.; Li, R. Efficient inhibition of Salmonella on chestnuts via Fe_3C/N-C bacteriostatic suspension prepared by electrochemical method. *Inorg. Chem. Commun.* **2020**, *118*, 108034. [CrossRef]

19. Miao, F.; Cui, P.; Yu, S.; Gu, T. In situ fabrication of a 3D self-supported porous Ni-Mo-Cu catalyst for an efficient hydrogen evolution reaction. *Dalton Trans.* **2023**, *52*, 8654–8660. [CrossRef] [PubMed]
20. Wang, W.; Liu, L.; Leng, W.; Gong, Y. Coordination Polymer-Derived Fe_3N Nanoparticles for Efficient Electrocatalytic Oxygen Evolution. *Inorg. Chem.* **2021**, *60*, 12136–12150. [CrossRef] [PubMed]
21. Ji, S.; Yang, Y.; Zhou, Z.; Li, X.; Liu, Y. Photocatalysis-Fenton of Fe-doped g-C_3N_4 catalyst and its excellent degradation performance towards, RhB. *J. Water Process Eng.* **2021**, *40*, 101804. [CrossRef]
22. Zhao, J.; Weng, Y.; Xu, S.; Shebl, A.; Wen, X.; Yang, G. Protein-mediated synthesis of Fe_3N nanoparticles embedded in hierarchical porous carbon for enhanced reversible lithium storage. *J. Power Sources* **2020**, *464*, 228246. [CrossRef]
23. Wang, T.; Xu, L.; Sun, C.; Li, X.; Yan, Y.; Li, F. Synthesis of hierarchically structured Fe_3C/CNTs composites in a FeNC matrix for use as efficient ORR electrocatalysts. *RSC Adv.* **2023**, *13*, 3835–3842. [CrossRef] [PubMed]
24. Li, C.; Zhang, R.; Ba, X.; Jiang, X.; Yang, Y. Fe Nanoparticles Encapsulated in N-Doped Porous Carbon for Efficient Oxygen Reduction in Alkaline Media. *J. Electrochem.* **2023**, *29*, 2210241.
25. Tang, F.; Lei, H.; Wang, S.; Wang, H.; Jin, Z. A novel Fe-N-C catalyst for efficient oxygen reduction reaction based on polydopamine nanotubes. *Nanoscale* **2017**, *9*, 17364–17370. [CrossRef]
26. Li, Y.; Yan, Y.; Ming, H.; Zheng, J. One-step synthesis Fe_3N surface-modified Fe_3O_4 nanoparticles with excellent lithium storage ability. *Appl. Surf. Sci.* **2014**, *305*, 683–688. [CrossRef]
27. Ding, M.; Jiang, W.; Yu, T.; Zhou, X.; Qin, X.; Yin, X. Electronically Modulated FeNi Composite by CeO_2 Porous Nanosheets for Water Splitting at Large Current Density. *J. Electrochem.* **2023**, *29*, 2208121.
28. Lai, Y.; Chen, W.; Zhang, Z.; Qu, Y.; Gan, Y.; Li, J. Fe/Fe_3C decorated 3-D porous nitrogen-doped graphene as a cathode material for rechargeable Li-O_2 batteries. *Electrochim. Acta* **2016**, *191*, 733–742. [CrossRef]
29. Eissa, A.; Peera, S.; Kim, N.; Lee, J. g-C_3N_4 templated synthesis of the Fe_3C@NSC electrocatalyst enriched with Fe–Nx active sites for efficient oxygen reduction reaction. *J. Mater. Chem. A* **2019**, *7*, 16920–16936. [CrossRef]
30. Wang, X.; Nan, Z. Highly efficient Fenton-like catalyst Fe-g-C_3N_4 porous nanosheets formation and catalytic mechanism. *Sep. Purif. Technol.* **2020**, *233*, 116023. [CrossRef]
31. Wang, C.; Yang, Q.; Li, Z.; Lin, Z.; Tong, S. A novel carbon-coated Fe-C/N composite as a highly active heterogeneous catalyst for the degradation of Acid Red 73 by persulfate. *Sep. Purif. Technol.* **2019**, *213*, 447–455. [CrossRef]
32. Liu, C.; Liu, L.; Tian, X.; Wang, Y.; Li, R.; Zhang, Y.; Song, Z.; Xu, B.; Chu, W.; Qi, F.; et al. Coupling metal-organic frameworks and g-C_3N_4 to derive Fe@N-doped graphene-like carbon for peroxymonosulfate activation: Upgrading framework stability and performance. *Appl. Catal. B-Environ.* **2019**, *255*, 117763. [CrossRef]
33. Ma, J.; Yang, Q.; Wen, Y.; Liu, W. Fe-g-C_3N_4/graphitized mesoporous carbon composite as an effective Fenton-like catalyst in a wide pH range. *Appl. Catal. B Environ.* **2017**, *201*, 232–240. [CrossRef]
34. Wang, Y.; Gao, C.; Zhang, Y.; Leung, M.; Liu, J.; Huang, S.; Liu, G.; Li, J.; Zhao, H. Bimetal-organic framework derived CoFe/NC porous hybrid nanorods as high-performance persulfate activators for bisphenol a degradation. *Chem. Eng. J.* **2021**, *421*, 11. [CrossRef]
35. Yu, D.; He, J.; Xie, T.; Xu, Q.; Li, G.; Du, L.; Huang, J.; Yang, J.; Li, W.; Wang, J. Peroxymonosulfate activation using a composite of copper and nickel oxide coated on SBA-15 for the removal of sulfonamide antibiotics. *Environ. Res.* **2022**, *206*, 11. [CrossRef] [PubMed]
36. Chen, X.; Han, Y.; Gao, P.; Li, H. New insight into the mechanism of electro-assisted pyrite minerals activation of peroxymonosulfate: Synergistic effects, activation sites and electron transfer. *Sep. Purif. Technol.* **2021**, *274*, 118817. [CrossRef]
37. Anipsitakis, G.; Dionysiou, D. Radical generation by the interaction of transition metals with common oxidants. *Environ. Sci. Technol.* **2004**, *38*, 3705–3712. [CrossRef] [PubMed]
38. Wang, L.; Li, J.; Liu, X.; Zhang, J.; Zeng, P.; Song, Y. Overestimation of $^1O_2$ role in N-doped carbon materials/peroxymonosulfate system: The misleading of furfuryl alcohol quenching effect. *Chemosphere* **2023**, *324*, 138264. [CrossRef]
39. Wang, Y.; Wang, S.; Liu, Y.; Wang, J. Peroxymonosulfate activation by nanocomposites towards the removal of sulfamethoxazole: Performance and mechanism. *Chemosphere* **2024**, *353*, 141586. [CrossRef] [PubMed]
40. Song, W.; Xiao, X.; Wang, G.; Zhang, X. Highly efficient peroxymonosulfate activation on Fe-N-C catalyst via the collaboration of low-coordinated Fe-N structure and Fe nanoparticles for enhanced organic pollutant degradation. *J. Hazard. Mater.* **2023**, *455*, 131596. [CrossRef]
41. Zhang, X.; Gu, W.; Liu, D.; Zhou, L.; Huy, N.; Wang, L.; Zhang, J.; Liu, Y.; Lei, J. Fe(II) and Pyridinic N complex sites synergy to activate PMS for specific generation of $^1O_2$ to degrade antibiotics with high efficiency. *Sci. Total Environ.* **2023**, *892*, 164067. [CrossRef] [PubMed]
42. Huang, M.; Wang, Y.; Wan, J.; Ma, Y.; Chi, H.; Xu, Y.; Qiu, S. Facile construction of highly reactive and stable defective iron-based metal organic frameworks for efficient degradation of Tetrabromobisphenol A via persulfate activation. *Environ. Pollut.* **2020**, *256*, 113399. [CrossRef] [PubMed]
43. Luo, T.; Wan, J.; Ma, Y.; Wang, Y.; Wan, Y. Sulfamethoxazole degradation by an Fe(II)-activated persulfate process: Insight into the reactive sites, product identification and degradation pathways. *Environ. Sci. Process Impacts* **2019**, *21*, 1560–1569. [CrossRef] [PubMed]

44. Du, J.; Guo, W.; Che, D.; Ren, N. Weak magnetic field for enhanced oxidation of sulfamethoxazole by Fe-0/H_2O_2 and Fe-0/persulfate: Performance, mechanisms, and degradation pathways. *Chem. Eng. J.* **2018**, *351*, 532–539. [CrossRef]
45. Liu, L.; Lin, S.; Zhang, W.; Farooq, U.; Shen, G.; Hu, S. Kinetic and mechanistic investigations of the degradation of sulfachloropyridazine in heat-activated persulfate oxidation process. *Chem. Eng. J.* **2018**, *346*, 515–524. [CrossRef]